3

Dynamics

The research on diesel engine transient operation has primarily focused on the relevant thermodynamic processes because of their direct impact on heat release and consequently performance and pollutants emissions. On the other hand, issues concerning (engine) dynamics are often over-simplified. Such notable dynamic issues that contribute to the non-linearity and complexity of diesel engine transient operation are

- development of the various forces of the slider-crank mechanism that may lead to considerable stress of the engine bearings;
- crankshaft torsional deformation resulting from the different magnitude of instantaneous torque values induced by the engine and load;
- governor clutch movement determining the actual fuel pump rack position;
- development of engine friction; and
- other dynamic issues induced by the whole vehicle propulsion.

3.1 Engine Dynamics

3.1.1 Kinematics and Forces of the Slider-crank Mechanism

At each instant of time, the displacement of the piston from the top dead center (TDC) position is given by the following equation with reference to Figure 3.1

$$x(\varphi) = r\left(1-\cos\varphi\right) + L_{rod}\left(1-\sqrt{1-\lambda^2\sin^2\varphi}\right) \tag{3.1}$$

where r=S/2 is the crank radius and $\lambda=r/L_{rod}$ with L_{rod} the connecting rod length.

Differentiating the above equation with respect to time, we get the instantaneous piston velocity

$$u_{pist}(\varphi) = \omega r \sin\varphi \left(1 + \frac{\lambda \cos\varphi}{\sqrt{1-\lambda^2 \sin^2\varphi}} \right) \tag{3.2}$$

and differentiating once again with respect to time, we get the instantaneous piston (linear) acceleration

$$b(\varphi) = \omega^2 r \left(\cos\varphi + \lambda \frac{\cos 2\varphi + \lambda^2 \sin^4\varphi}{(1-\lambda^2 \sin^2\varphi)^{3/2}} + \frac{1}{\omega^2} \varepsilon \frac{u_{pist}(\varphi)}{r\omega} \right) \tag{3.3}$$

The last term on the right-hand side of Equation 3.3 accounts for the influence of the crank's angular acceleration $\varepsilon = d\omega/dt$ on the piston linear acceleration. Further, the connecting rod angle β is given by

$$\sin\beta = \lambda \sin\varphi \Leftrightarrow \beta = \cos^{-1}\left(\sqrt{1-\lambda^2 \sin^2\varphi} \right) \tag{3.4}$$

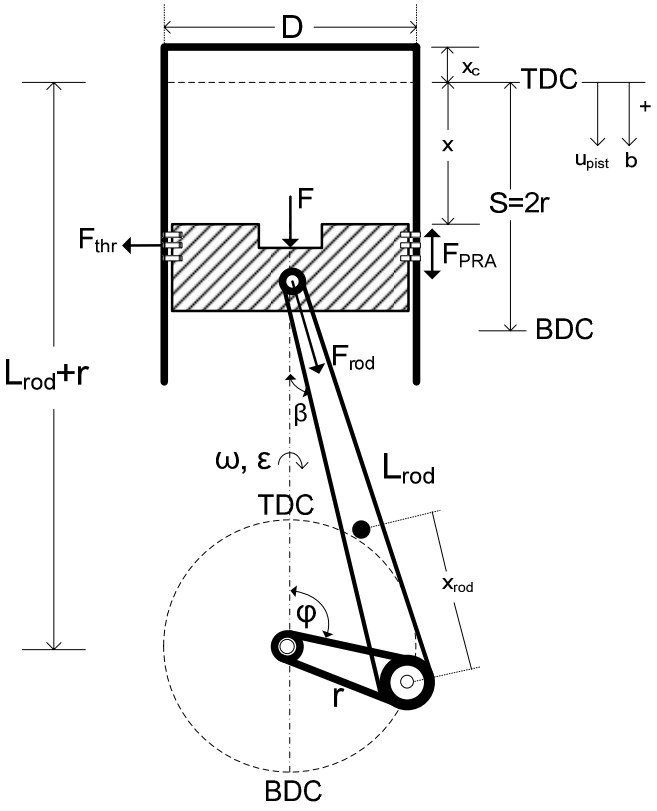

Figure 3.1. Schematic diagram of slider-crank mechanism

Total force acting on the piston comprises of thermodynamic and inertia terms

$$F(\varphi) = F_g(\varphi) + F_{in}(\varphi) = p_g(\varphi)A_{pist} - m_l b(\varphi) = p_g(\varphi)A_{pist} - m_l r\omega^2 \left(b(\varphi)/r\omega^2\right) \quad (3.5)$$

This force propagates into the thrust force $F_{thr}(\varphi) = F(\varphi)\tan\beta$ and the force in the direction of the connecting rod $F_{rod}(\varphi) = F(\varphi)/\cos\beta$. Also, A_{pist} is the piston surface area = $\pi D^2/4$. Piston rings assembly friction force F_{PRA} in Figure 3.1 will be discussed in Section 3.3.

The reciprocating mass m_l in Equation 3.5 is given by

$$m_l = m_{pist} + m_{rod.l} \quad (3.6a)$$

whereas for the rotating masses

$$m_r = m_{rod.r} + m_{crank.eq} \quad (3.6b)$$

In the above equations, m_{pist} is the mass of the piston assembly (piston, rings, wrist pin) and $m_{crank.eq}$ is the equivalent rotating mass of the crank with reference to the crankpin.

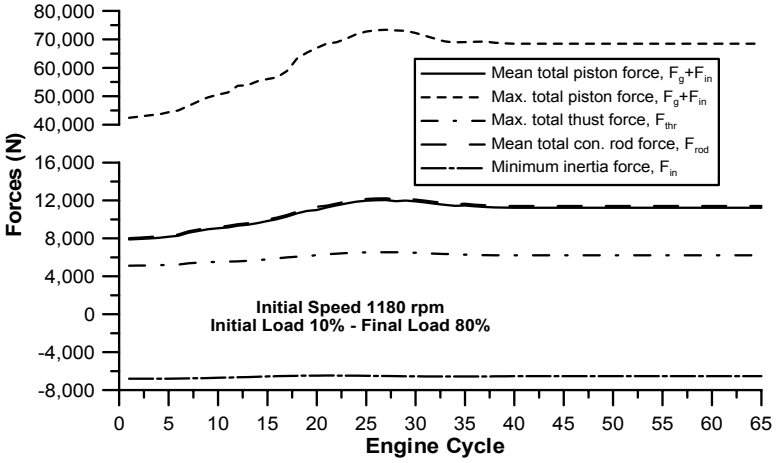

Figure 3.2. Mean and maximum, over each engine cycle, slider-crank mechanism forces during a 10–80% load increase transient event ('total' denotes the sum of gas and inertia forces contribution)

The connecting rod is usually assumed equivalent to two masses, one reciprocating with the piston assembly $m_{rod.l}$ and the other rotating with the crank $m_{rod.r}$. The following two equations apply with reference to Figure 3.1:

$$m_{rod} = m_{rod.r} + m_{rod.l} \quad (3.7a)$$

$$m_{rod.l}(L_{rod} - x_{rod}) = m_{rod.r}\, x_{rod} \tag{3.7b}$$

with x_{rod} the distance between the connecting rod's center of gravity and its big end bearing and m_{rod} the connecting rod mass. It follows then that $m_{rod.r} x_{rod}^2 + m_{rod.l}(L_{rod} - x_{rod})^2 \neq G_{rod}$ with G_{rod} the real connecting rod mass moment of inertia; the difference is, however, usually negligible.

Figure 3.2 illustrates the development of some mean and maximum, over each engine cycle, slider-crank mechanism forces during a 10–80% load increase transient event of a turbocharged diesel engine. Clearly, thrust forces are always of much less importance owing to the small connecting rod angles involved, and the same holds true for inertia forces (notice the negative sign, actually denoting the minimum rather than the maximum value of this force). The latter are not so pronounced for the particular operating case depicted in Figure 3.2 owing to the relatively low engine speed (recall that inertia forces depend on the engine speed squared).

For the loading of the slider-crank mechanism bearings, the following equations can be developed with reference to Figure 3.3:

$$B_{0x} = -m_{rod.l} \cdot b \sin\beta \quad , \quad B_{0y} = -\frac{F(\varphi)}{\cos\beta} - m_{rod.l} \cdot b \cos\beta \tag{3.8}$$

for the connecting rod small end bearing,

$$B_{1x} = -m_{rod.r} \cdot u_{pist} \cdot \omega \cdot \cos\beta \quad , \quad B_{1y} = \frac{F(\varphi)}{\cos\beta} - m_{rod.r} \cdot r\omega^2 \cos(\varphi + \beta) \tag{3.9}$$

for the connecting rod big end bearing,

$$B_{2x} = \frac{F(\varphi)}{\cos\beta}\sin(\varphi + \beta) \quad , \quad B_{2y} = -\frac{F(\varphi)}{\cos\beta}\cos(\varphi + \beta) + m_{rod.r} \cdot r\omega^2 \tag{3.10}$$

for the crank pin (single cylinder contribution),

$$B_{3x} = -\frac{1}{2}\frac{F(\varphi)}{\cos\beta}\sin(\varphi + \beta) \quad , \quad B_{3y} = \frac{1}{2}\left[\frac{F(\varphi)}{\cos\beta}\cos(\varphi + \beta) - m_r r\omega^2\right] \tag{3.11}$$

for the crank journal (single cylinder contribution), and

$$\begin{aligned} B_{4x} &= \frac{1}{2}\left[F(\varphi)\tan\beta + m_r r\omega^2 \sin(\varphi)\right] \\ B_{4y} &= \frac{1}{2}\left[-F(\varphi) + m_r r\omega^2 \cos(\varphi)\right] \end{aligned} \tag{3.12}$$

for the main crankshaft bearing (single cylinder contribution).

The corresponding total bearing force is then given for each case by

$$B_i = \sqrt{B_{ix}^2 + B_{iy}^2} \tag{3.13}$$

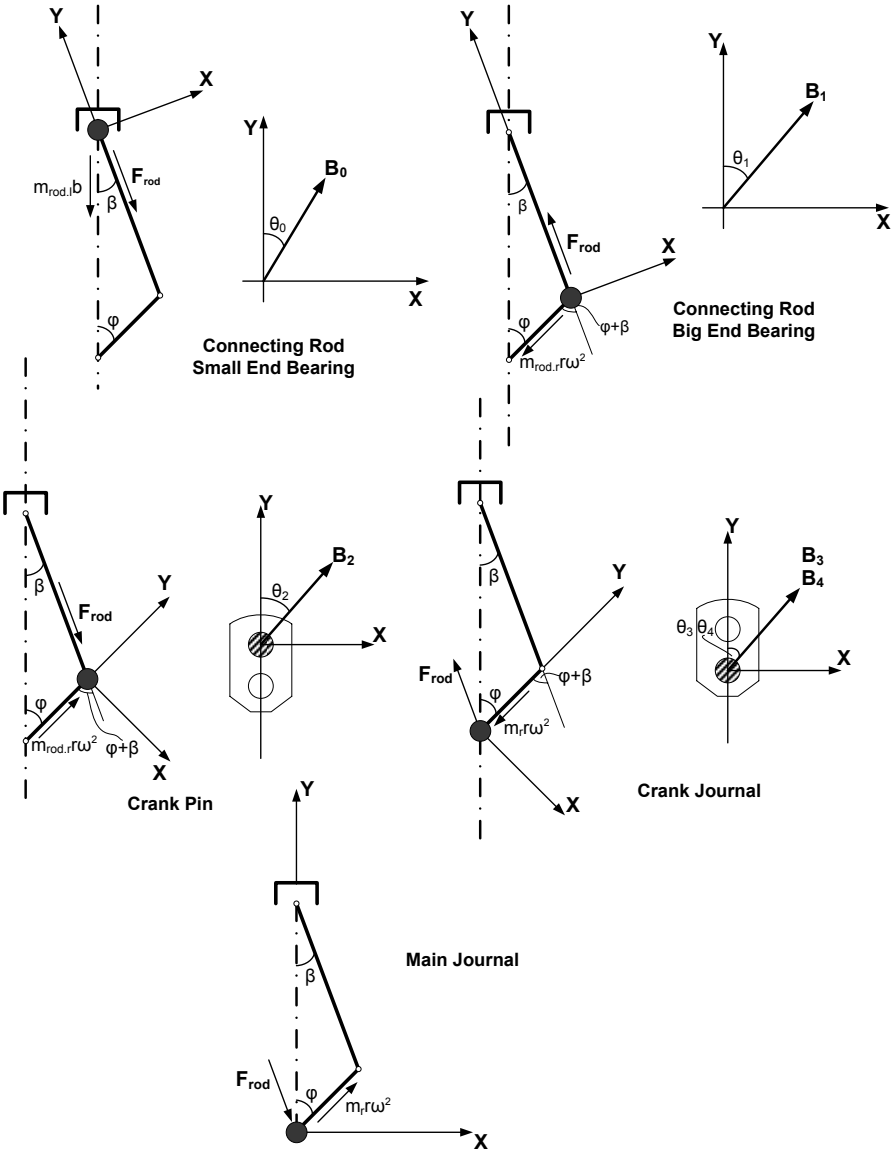

Figure 3.3. Forces distribution for bearing loadings evaluation [1]

and the angle θ, shown in Figure 3.3 is calculated from

$$\theta_i = \tan^{-1}\left(\frac{B_{ix}}{B_{iy}}\right) \tag{3.14}$$

with i = 0…4 according to the bearing under study.

Figure 3.4 illustrates the development of maximum bearing loadings during the same 10–80% transient step load increase. The response of piston force ($F_g(\varphi) = p_g(\varphi)\, A_{pist}$), engine speed and fueling are also depicted in the same figure for comparison purposes.

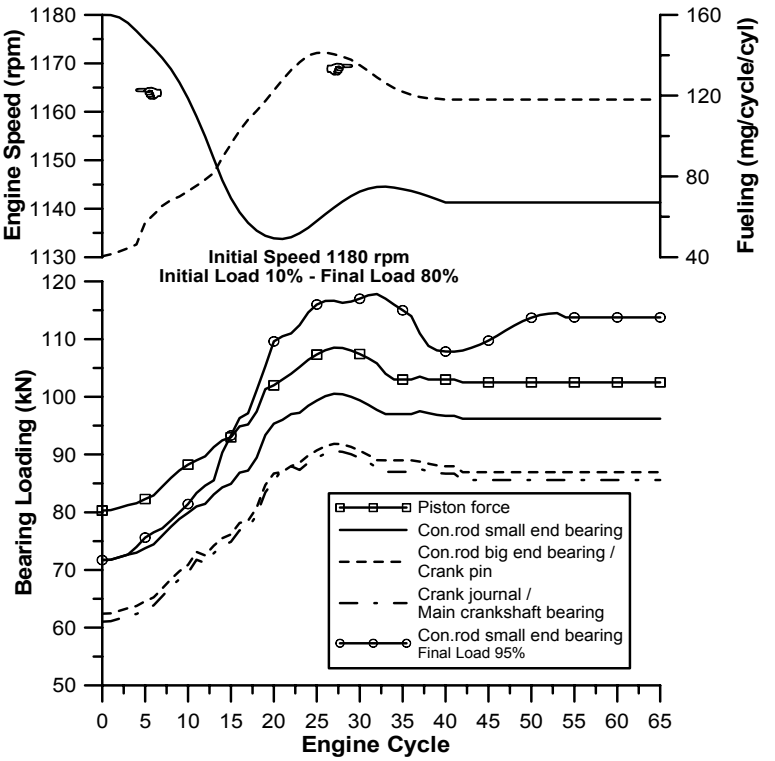

Figure 3.4. Maximum bearing loadings *vs.* engine cycle for a 10–80% load increase transient event

The main findings derived from Figure 3.4 are summarized below.

- Maximum values, over each engine cycle, of all bearing loadings develop during a transient event in a way that closely follows the fueling and the peak cylinder pressure profiles owing to the dominance of gas pressures on the B_i terms.

- Turbocharger lag effect is obvious during the first cycles of the transient event.
- The connecting rod's big end bearing loading equals the crank pin's one, whereas the crank journal's loading equals the main crankshaft bearing's one.
- Loading gradually decreases as we move downwards the kinematics mechanism, *i.e.,* from the piston towards the crankshaft, as the initial (gas) force is 'propagated'.
- Contribution of inertia forces is minimal (as regards maximum (absolute) values only), primarily due to the low engine rotational speed (*cf.* the ω^2 term in Equations 3.9–3.12).

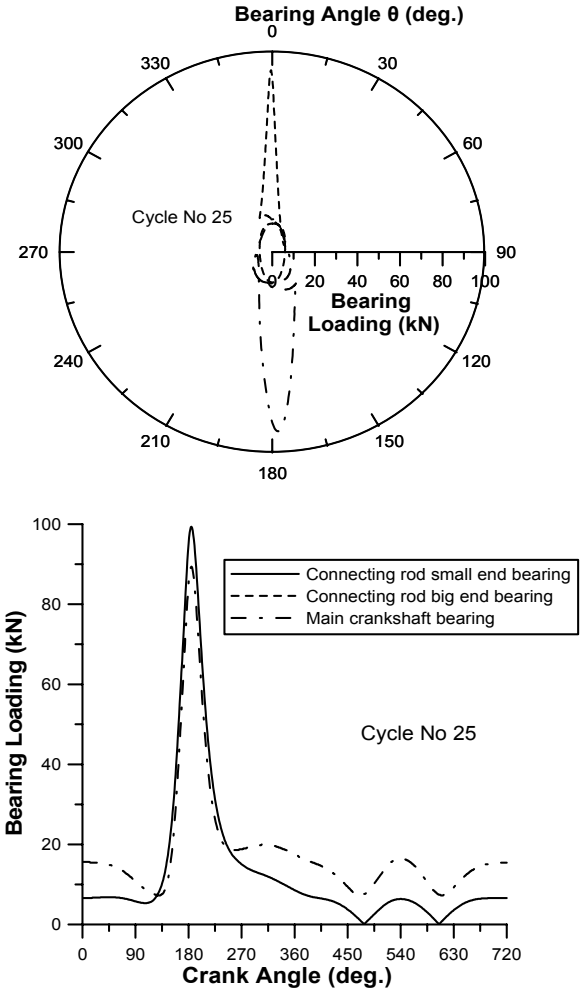

Figure 3.5. Development of connecting rod and main crankshaft bearing loadings during an intermediate cycle of a 10–80% load increase transient event [1]

- The crank angle where the maximum loading is observed ranges for all bearings and for all transient cycles from 1–4°CA after firing TDC, as is also the case with the peak cylinder pressure for the particular engine.
- As regards loading rate, the maximum increase is observed between cycles 10–30 where the main part of the increase in fueling occurs; it is of the order of 16 kN/s for the specific 10–80% load increase transient.

Figure 3.5 focuses on an intermediate cycle of the transient event (cycle No. 25, where maximum fueling occurs), illustrating the in-cycle build-up of the connecting rod and main crankshaft bearing loadings. The contribution of gas force is evident during the compression and expansion strokes; however, it is the inertia force $F_{in}(\varphi)$ that defines the loading profile during most of the open part of the cycle, where the cylinder pressure assumes lower values. In the upper diagram of Figure 3.5 the above data are illustrated on a polar diagram, which is a more common way of depiction in terms of this kind of analysis.

Lee *et al.* [2] investigated experimentally the thermal and load stress during various transient schedules (starting, shutting down, changing load at constant engine speed); consistent with the results presented in the previous figures, they concluded that although the force/loading levels increase significantly with increasing load, the actual values of the mechanical stress during transients are only marginally higher than those corresponding to the respective steady-state conditions.

3.1.2 Crankshaft Torque Balance

In the general case, the crankshaft is assumed to be a flexible, elastic body that may deform during engine operation; the lumped mass model of Figure 3.6 can be employed. This illustrates a condensed (crank)shaft model, *i.e.,* rigid enough between the cylinders and elastic between flywheel and load. The elastic crankshaft rotary motion is excited by the gas and inertia force fluctuation. The rotary motion of the shaft is expressed by the following two differential equations describing its angular momentum balance based on Newton's second law of motion:[1]

$$\tau_e(\varphi) - \tau_{fr}(\varphi) - \tau_S - \tau_D = G_e \frac{d\omega}{dt} + \frac{1}{2}\frac{\partial G_e(\varphi)}{\partial \varphi}\left(\frac{d\varphi}{dt}\right)^2 \tag{3.15a}$$

$$\tau_S + \tau_D - \tau_L(\varphi_L) = G_L \frac{d\omega_L}{dt} \tag{3.15b}$$

In Equations 3.15, G_e is the engine (see next section) and G_L is the load (resistance) mass moment of inertia, respectively.

[1] Sir Isaac Newton's (1642–1727) formulation of second law of motion for rotational systems states that the sum of torques acting on a body about a given axis is equal to the product of its rotational moment of inertia and the rotational acceleration about the axis.

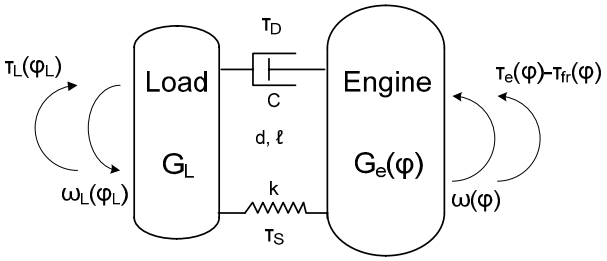

Figure 3.6. Schematic arrangement of the engine-load dynamic system for crankshaft torque balance analysis

Also, $\omega=d\varphi/dt$ is the engine angular velocity and $\omega_L = d\varphi_L/dt$ is its load counterpart. Further, $\tau_{fr}(\varphi)$ is the total (from all cylinders) friction torque and $\tau_e(\varphi) = \sum_{i=1}^{n_{cyl}} \tau_{ei}(\varphi)$ denotes the total engine indicated torque that includes the contribution of gas, inertia and (the negligible) gravitational forces. Individual cylinder indicated torque $\tau_{ei}(\varphi)$ is given explicitly by

$$\tau_e(\varphi) = \overbrace{\tau_g(\varphi)}^{\text{Gas}} + \overbrace{\tau_{in}(\varphi)}^{\text{Inertia}} + \overbrace{\tau_{gr}(\varphi)}^{\text{Gravitational}} = \left[\overbrace{\left(p_g(\varphi)\, A_{pist}\, \frac{u_{pist}(\varphi)}{r\omega} \right)}^{\text{Gas}} - \overbrace{\left(m_l\, b(\varphi)\, \frac{u_{pist}(\varphi)}{r\omega} \right)}^{\text{Inertia}} + \overbrace{\left(m_l\, g\, \frac{u_{pist}(\varphi)}{r\omega} + m_r\, g\, \sin\varphi \right)}^{\text{Gravitational}} \right] r \tag{3.16}$$

with $p_g(\varphi)$ the instantaneous cylinder gas pressure and g the gravitational acceleration.[2]

For the torsional stiffness and damping torques we have, respectively,

$$\tau_S = k\,(\varphi - \varphi_L) \tag{3.17}$$

$$\tau_D = C\,(\omega - \omega_L) \tag{3.18}$$

with k the shaft stiffness coefficient, and C the damping factor (Figure 3.6).

In most of the cases, however, the crankshaft can be assumed short and rigid enough, hence, $\varphi \equiv \varphi_L$ and $\omega \equiv \omega_L$. Then, by adding both sides of Equations 3.15, these are replaced by the following much simpler equation:

$$\tau_e(\varphi) - \tau_{fr}(\varphi) - \tau_L(\varphi) = G_{tot}\, \frac{d\omega}{dt} \tag{3.19}$$

[2] For the calculation of total engine torque at the flywheel end, the crank angle difference between successive firing cylinders is required in order to formulate n_{cyl} equations similar to 3.16.

where G_{tot} represents the total mass moment of inertia of the engine–load configuration reduced to the crankshaft axis.

For the resistance torque term, τ_L in Equations 3.15b and 3.19, the following relation can be applied (for small speed changes):

$$\tau_L(\omega_L) = C_1 + C_2\omega_L^{C_3} \tag{3.20}$$

- for a linear load-type (electric brake, generator) C_3=1;
- for a quadratic load-type (hydraulic brake, fixed pitch propeller, vehicle aerodynamic resistance) C_3=2; and
- C_1 is the speed-independent load term (*e.g.,* road slope – see Section 3.5).

An even more detailed angular momentum balance can be formulated by taking into account all possible crankshaft deformations between pulley, each cylinder (or crank) of a multi-cylinder diesel engine, flywheel and load. This eventually leads to a system of multiple differential equations (similar to those given in Equations 3.15), depending on the number of cylinders (cranks) of the engine in question, as it is depicted in Figure 3.7 for a six-cylinder engine.

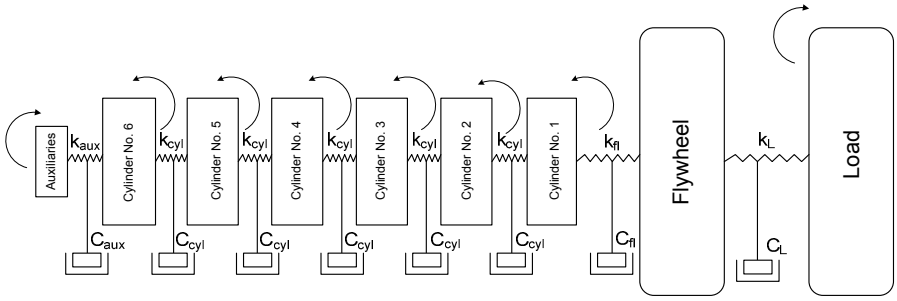

Figure 3.7. Schematic arrangement of detailed engine–load dynamic system of an in-line six-cylinder engine

However, as was shown by Rakopoulos *et al.* [1] the results from such detailed crankshaft torque balance in terms of engine rotational speed calculation are only marginally different from the simplified Equation 3.19.

3.1.3 Mass Moments of Inertia

The total engine mass moment of inertia G_e needed in the crankshaft torque balance analysis of the previous section is calculated from the following equation

$$G_e = G_{fl} + G_{coupl} + n_{cyl}(G_r + G_l) + G_{var} \tag{3.21a}$$

Here, the total engine inertia includes flywheel G_{fl} and, if applicable, elastic coupling G_{coupl} contribution, with n_{cyl} the number of engine cylinders and G_{var} other engine-based terms such as gears, pulleys *etc.;* G_l is the varying, according to crank angle, reciprocating masses inertia reduced to the crankshaft axis, given by

$$G_l = m_l r^2 \left(\frac{u_{pist}(\varphi)}{r\omega} \right)^2 \tag{3.21b}$$

and G_r is the rotating masses moment of inertia, which according to Figure 3.8 is computed by

$$G_r = \overbrace{G_w + \left(G_{Kr} + m_K r^2\right) + 2G_B}^{\text{Crank assembly}} + G_{rod.r} = \underbrace{\frac{\pi}{32}\rho d_w^4 \ell_w}_{\text{Crank journal}} + \underbrace{\left(\frac{\pi}{32}\rho d_K^4 \ell_K \left(d_K^2 + 8r^2\right) \right)}_{\text{Crank pin}} + \underbrace{2G_B}_{\text{Crank cheeks}} + \underbrace{m_{rod.r}\, r^2}_{\substack{\text{Connecting rod} \\ \text{big end bearing}}} \approx m_r r^2 \tag{3.21c}$$

with m_r defined in Equation 3.6b, and ρ the material density. Ideally, the counterweights moment of inertia should be taken into account in Equation 3.21c.

Further, by substituting the $u_{pist}(\varphi)$ term from Equation 3.2, into Equation 3.21b, we get

$$\bar{G}_l = \left(\frac{1}{2} + \frac{\lambda^2}{8} + ...\right) m_l r^2 \approx \frac{1}{2} m_l r^2 \tag{3.21d}$$

which can be used as a very good approximation for the mean, over an engine cycle, reciprocating masses moment of inertia.

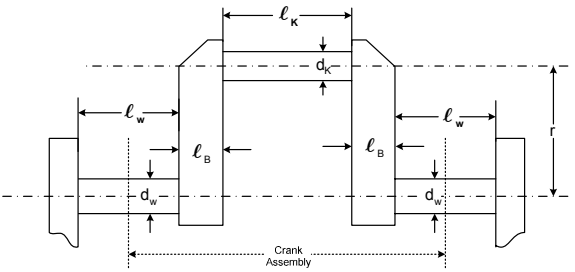

Figure 3.8. Schematic arrangement of crank for calculation of rotating masses moment of inertia

3.2 Governor

3.2.1 Governor Fundamentals

Unlike spark ignition engines, the diesel engine's fuel pump curves are characterized by increasing values with increasing engine speed. Even a slight

increase in speed from the equilibrium conditions leads to increase in the injected fuel quantity, hence engine torque. At idling conditions (without speed regulation), engine speed would either increase constantly or decrease to stall. Likewise, after cold starting and while the engine operates at idling conditions, engine speed would constantly rise due to the gradual decrease in resistance and friction torque during warm-up. Hence, the diesel engine, being inherently unstable, particularly at low loads and speeds, requires some kind of feedback control in order to maintain engine speed. This control is realized through the speed governor that determines fueling consistent with current engine operating conditions and requested changes in desired engine speed.

In order to understand the mechanism behind the governor control we need to look back into the angular momentum balance of the engine crankshaft (Equation 3.19). Since friction and resistance torque are, mainly, dependent on engine speed, and, in general, $\tau_e \propto \eta_e \dot{m}_{fi}$, with η_e the engine brake efficiency, it is made obvious that in order to manipulate speed the only engine variable that can be externally regulated is the injected fuel quantity $\dot{m}_{fi}$; this regulation is achieved through the speed governor. Engine speed regulation is accomplished via negative feedback control, *i.e.,* decrease in engine speed causes increase in fueling. Figure 3.9 depicts the block diagram of the basic governor action.

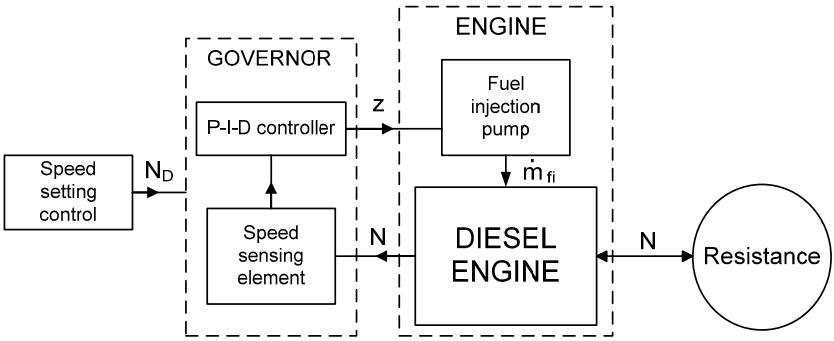

Figure 3.9. Block diagram of typical speed governor operation (N: actual engine speed, N_D: demand speed, $\dot{m}_{fi}$: injected fuel quantity, z: fuel pump rack position)

The desired or demand engine speed N_D (as dictated, for example, by the position of the accelerator pedal in passenger vehicles or as set by the governor control lever in industrial engines) and the actual engine speed N are the two basic inputs to the governor control loop. Any difference in the values of these two signals (*e.g.,* decrease in actual engine speed due to sudden load application) results in displacement of the governor sensing element; the latter alters the fuel pump rack position z, therefore the injected fuel quantity $\dot{m}_{fi}$, and engine torque τ_e in order to establish a new equilibrium between engine and resistance (load) at a different or even the same rotational speed.

Governors are either direct or indirect acting. Both types consist of a sensing element for the sensing of speed change; the indirect acting governors incorporate

also a servomechanism that is connected to the fuel pump rack, correcting the fueling. The sensing elements are usually mechanical (with flyweights) or electrical/electronic. Servomechanism feedback may be unity or vanishing; the vanishing feedback indirect acting governor achieves constant governing (zero speed droop after a load change) and is termed isochronous. On the other hand, direct acting governors are characterized by permanent speed droop according to the applied load change. Direct acting governors apply proportional (P) control, meaning that the change in injected fuel quantity is determined by the difference between actual and desired speed (power amplification). Isochronous governors incorporate proportional plus integral (P-I) control. Finally, a governor may apply differential control (P-I-D controller), in which case the fuel pump rack movement is also affected by the rate of change of engine speed. In mechanical fuel injection systems, the governor is a separate device, usually attached to the fuel pump casing (Figure 3.10), whereas in modern, common rail injection systems, the governor function is integrated in the engine control unit.

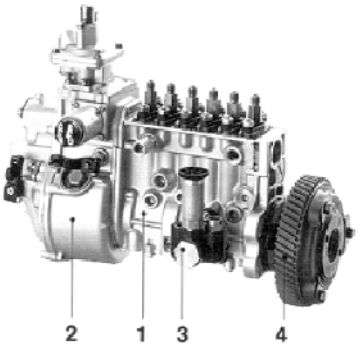

Figure 3.10. Mechanical in-line fuel pump incorporating a speed governor. 1: fuel injection pump; 2: governor; 3: fuel-supply pump; 4: timing device (reprinted with permission from Bosch [3])

Figure 3.11a describes in more detail the control loop of a conventional mechanical governor fitted on a vehicle engine; it emphasizes on its auxiliary functions, *i.e.,* fuel limiting (identified through the input signal of turbocharger compressor boost pressure, as was discussed in Section 2.2.2) as well as load regulation, starting requirements or altitude compensation (atmospheric pressure signal). Figure 3.11b illustrates the much more complex loop of a modern electronic governor integrated in the engine ECU receiving several signals from various sensors and processing them in a micro-processor.

If the governor regulates speed at a unique operating condition, for example idling, or maximum speed, it is called one-speed governor. A common type of automobile governor regulates speed at two distinct speeds, *i.e.,* idle and maximum speed and is termed a minimum/maximum governor. In Figure 3.12 this is accomplished via two springs of different stiffness, whereas in the middle of the operating range, engine output is directly affected by the accelerator pedal position, enhancing driveability. When the governor regulates speed over the whole engine operating range, it is termed all-speed or variable speed.

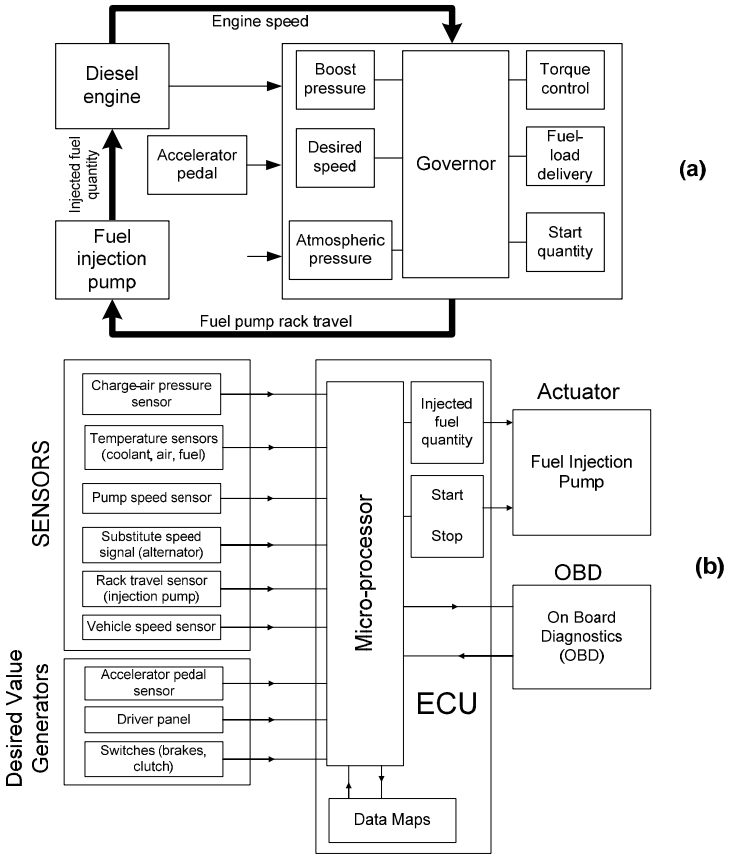

Figure 3.11. *a:* Mechanical governor closed-loop control of a vehicle engine. *b:* Electronic governor closed-loop control of a modern passenger vehicle engine (reprinted with permission from Bosch [3])

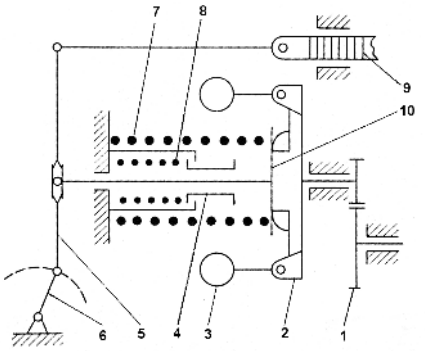

Figure 3.12. Min-max governor (1: step-up gear, 2: cross-piece, 3: flyweight, 4: support bushing, 5: lever, 6: control lever, 7: external spring, 8: internal spring, 9: fuel rack, 10: clutch) (from Krutov [4], reprinted with permission from the Russian Authors Society)

The characteristics of the governor depend upon the specific application. For example, the vanishing feedback indirect (isochronous) governor is ideal for electrical generation applications, where strict maintenance of engine rotational speed is desired irrespective of engine load (see also Figure 1.10). On the contrary, vehicular applications require less tight governing, otherwise the driveability of the vehicle would be impossible. Agricultural tractors, road-sweeping machines, ships *etc.,* use variable speed governors, which regulate speed over the whole engine operating range; for example in ships, a variable speed governor maintains each defined cruising speed.

In Figure 3.13, which illustrates a typical variable speed governor, the springs are incorporated into the flyweights; the latter move outward within the specified adjustment range as long as speed increases. Each control lever position is allocated a given speed at which regulation begins. Control lever movement is transmitted through the two piece linkage lever and the guide block to the variable fulcrum lever, and thus to the control rack.

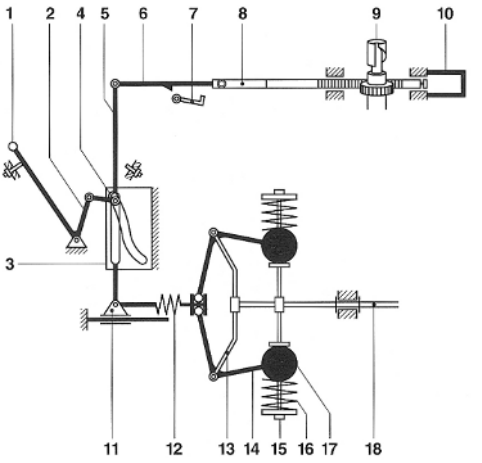

Figure 3.13. Variable speed governor (1: control lever, 2: linkage lever, 3: plate cam, 4: guide block, 5: fulcrum lever, 6: link fork, 7: full-load stop (automatic), 8: control rack, 9: pump plunger, 10: start quantity stop, 11: slider, 12: sliding bolt with drag spring, 13: governor hub, 14: bell crank, 15: adjustment nut, 16: governor spring, 17: flyweight, 18: camshaft) (reprinted with permission from Bosch [3])

Typical steady-state curves of a variable speed governor are illustrated in Figure 3.14. In addition to the low- and high-idle (maximum) speeds, this governor regulates intermediate speeds independent of engine load; the speed is set at the governor control lever. With reference to Figure 3.14, the engine starts with the start quantity determined through the automatic starting rack travel. During warm-up, low-idle speed finally levels off at point L. Full-load regulation follows the full-load curve, and torque control takes place between speeds N_1 and N_2 until speed regulation break-away starts at maximum full-load speed following the line from N_{vo} (maximum full-load speed) to N_{lo} (maximum speed). The remaining

curves show the break-away characteristics for the intermediate speeds, whereby the increase in speed droop for decreasing engine speed is evident [3].

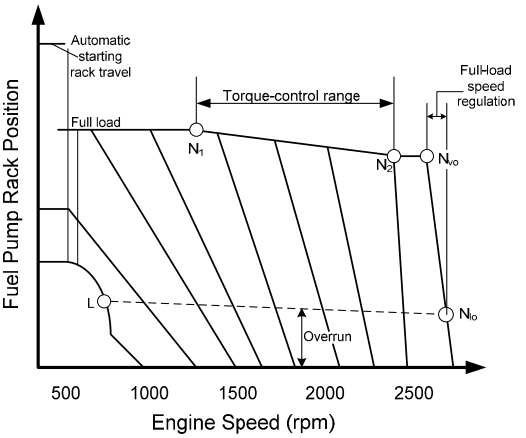

Figure 3.14. Steady-state curves of a mechanical variable-speed governor (reprinted with permission from Bosch [3])

Krutov [4], Welbourn *et al.* [5], Webb and Janota [6] and Catania *et al.* [7] discuss various issues concerning governor application and control under steady-state and transient conditions applying transfer function analysis. They also propose equations for modeling the various governor types, as they will be described briefly in the next sub-section. Rackmil and co-workers [8] discuss in detail the operation of an electro-hydraulic governor and its auxiliary functions (buffer system by-pass, compensation cut-off, load regulation and fuel limiting) for transient operation of a two-stroke, locomotive diesel engine applying quasi-linear engine modeling.

3.2.2 Governor Equations

A simple mechanical sensing element, following the Watt principle,[3] is illustrated in Figure 3.15. Here, the centrifugal force of the rotating flyweights (2) is opposed by the spring (9) force. In this sensing element the acting spring is located far from the flyweights and opposes their centrifugal force through the lever (10) motion.

The supporting, *i.e.,* centrifugal force of the flyweights for the mechanical sensing element of Figure 3.15 can be expressed by the following relation [4]:

$$F_{sup} = (a_{se} + b_{se} z)\, N_{gov}^2 \tag{3.22}$$

[3] James Watt (1736–1819) designed in 1787 a centrifugal governor to control the speed of a steam engine. Significant theoretical studies on governing were conducted during the second half of the 19th century by C. W. Siemens in 1853 and 1866, and James Clerk Maxwell (1831–1879); the latter presented in 1868 before the Royal Society of UK his classic work 'On governors' dealing with the equations of motion of a closed-loop system, such as the steam engine fitted with a Siemens governor.

where $a_{se} = (nm)_{fw}\,\ell \cdot r_o / d$ and $b_{se} = (nm)_{fw} \cdot (\ell / d)^2$ with n, m the number and mass of flyweights, respectively, d, ℓ, r_o are lengths as shown in Figure 3.15, z is the current displacement of clutch (8) ranging from 0 to z_{max} and $N_{gov}=i_{gov}$ N, with i_{gov} the transmission ratio between crankshaft and governor axis (typical value 0.5).

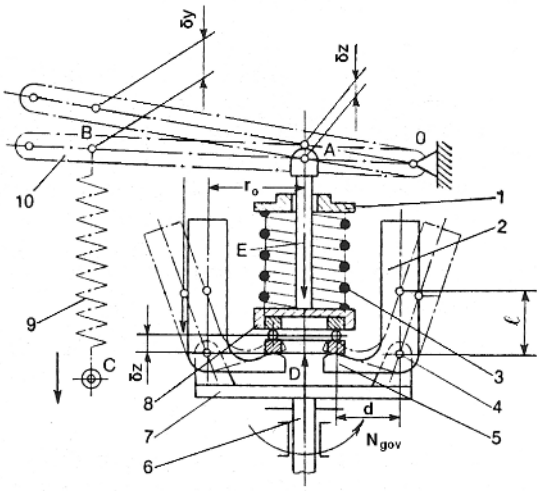

Figure 3.15. Mechanical speed sensing element (1: spring thrust plate, 2: flyweights, 3: spring alligned with clutch, 4: weight pivot, 5: lug, 6: governor shaft, 7: cross-piece, 8: clutch, 9: spring remote from clutch, 10: lever) (from Krutov [4], reprinted with permission from the Russian Authors Society)

The spring (9) restoring force is expressed as follows

$$F_{rest} = k\, i_{tr}\,(y + i_{tr} z) \tag{3.23}$$

where y is the (constant) prior spring strain (a measure of 'throttle position', often referred to as the 'governor setting') made possible either by moving thrust plate (1) or point C of spring (9), k is the spring stiffness (constant or varying with engine speed for conical springs with square-law characteristics) and $i_{tr}=\delta y_B/\delta z$ is the transmission ratio of the mechanism coupling the clutch (8) with the spring (9) by means of lever OB. For $i_{tr}=1 \Rightarrow \delta y_B \equiv \delta z$, which means that the restoring spring deformation is equal to the displacement z of the clutch (8). At steady-state conditions the above mentioned two forces are in equilibrium, so that it holds (neglecting the weight of ballarms and clutch) that

$$F_{sup} = F_{rest} \Leftrightarrow z = \frac{a_{se}\, i_{gov}^2\, N_{gov}^2 - k\, i_{tr}\, y}{k\, i_{tr}^2 - b_{se}\, i_{gov}^2\, N^2} \tag{3.24a}$$

For an electrical sensing element the supporting force is electromagnetic; a core of known reluctance and cross section area plays the role of the flyweights. A voltage

is applied at its ends proportional to the current angular velocity ω of the engine. Speed changes are transformed into voltage changes and the core pushes the spring or is being pushed by it. Equation 3.22 holds true again, but now a_{se} is a function of core reluctance, cross section area and gain factor between engine speed and induced voltage at the core edges; b_{se} on the other hand equals zero. By altering the prior spring strain y, one manipulates the sensing element equilibrium curve (3.24a), the initial operating point and, thus, the whole engine speed response.

As with almost all aspects of transient operation, the governor steady-state curves (Figure 3.14 or Equation 3.24a) differentiate during a load or speed change. During transient operation, Newton's second law of motion for the mechanical sensing element of Figure 3.15 states

$$\underbrace{F_{sup}}_{\text{Supporting force}} + \underbrace{F_{2p}}_{\text{2 pulse term}} - \underbrace{F_{rest}}_{\text{Spring force}} - \underbrace{f_{gov}\frac{dz}{dt}}_{\text{Friction}} = \underbrace{m_{gov}\frac{d^2z}{dt^2}}_{\text{Acceleration}} \tag{3.24b}$$

where f_{gov} is the friction coefficient in Ns/m of the governor clutch (mainly a function of its speed) and m_{gov} is the mass of clutch and flywheels.

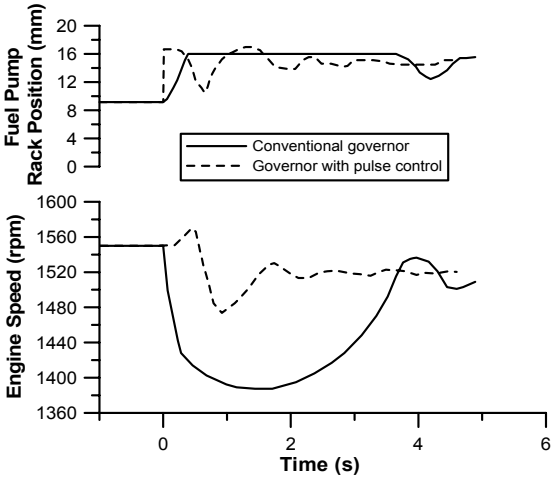

Figure 3.16. Effect of pulse governor (differential control) on the transient performance of a 12 cylinder turbocharged diesel engine driving an electrical generator (reprinted with permission from Zellbeck and Woschni [9])

The term F_{2p} ($=A_{2p}\varepsilon\, i_{gov}$ N) exists only for a *two-pulse* sensing element, *i.e.,* one which responds not only to the angular velocity variations but also to the crankshaft angular acceleration ones (this kind of feedback was defined in Section 3.2.1 as differential control). It can, therefore, prove very effective for improving engine maximum speed droop, although it may lead to an unstable recovery (Figure 3.16). At steady-state conditions it behaves as an ordinary mechanical sensing element being governed by the same equilibrium Equation 3.24a, though at transient conditions the second term on the left-hand side of Equation 3.24b

appears (since angular acceleration $\varepsilon \neq 0$); term A_{2p} depends on the design of the ballhead and its mass moment of inertia.

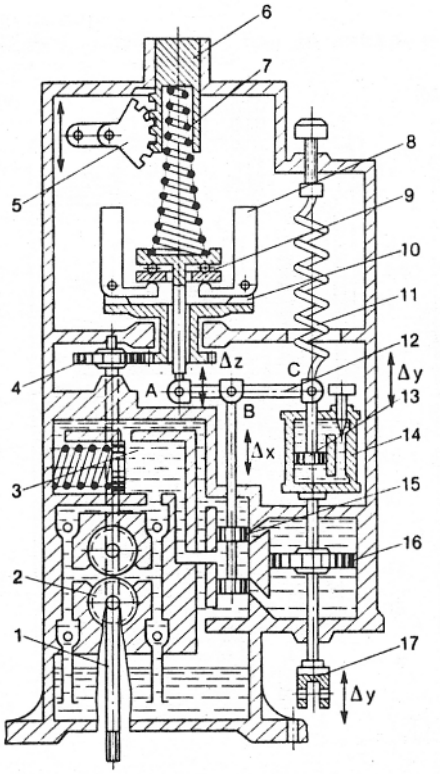

Figure 3.17. Isochronous governor with P-I feedback (1: driving shaft, 2: oil pump, 3: oil pressure accumulator, 4: driving gear, 5: spring prior strain variator, 6: spring upper support, 7: spring, 8: flyweight, 9: clutch, 10: cross-piece, 11: P-I element spring, 12: feedback lever, 13: P-I element piston, 14: P-I element, 15: control valve, 16: servopiston, 17: rod) (from Krutov [4], reprinted with permission from the Russian Authors Society)

Indirect acting governors, whether of unity or vanishing feedback, almost exclusively make use of hydraulic servomotors as power elements and are usually equipped with mechanical sensing elements. In cases where a governor must ensure a strictly constant engine speed irrespective of load, vanishing feedback is applied, which is a proportional plus integral (P-I) controller (Figure 3.17 with $i_{tr}=1$ for the sensing element). Depending on the load applied, piston (16) and rod (17), coupled with the rack, occupy distinct positions under the steady-state conditions, whereas point C is moved to its initial position by means of spring (11) when the transient terminates. Since point B of lever (12) occupies one and always the same position under all steady-state conditions, point A, coupled with clutch (9) of the sensing element, must also occupy one and the same position under all steady-state conditions. This may happen only at one and the same angular velocity, set by

support (6), which occupies a permanent position. Thus, after a load change, restoration of speed is achieved to its initial value [4].

Rakopoulos *et al.* [10] based on the above analysis of Krutov [4], modeled several governor sensing elements and feedbacks; they coupled the analysis with a comprehensive, filling and emptying transient simulation code for a single cylinder, naturally aspirated diesel engine operating under load increase transients. Their analysis revealed the facts detailed below.

- Geometrical and technical characteristics of the governor affect the engine response seriously in terms of speed droop, recovery period and whole speed response profile. The impact of each term, however, was sometimes conflicting when comparing speed droop and recovery period.
- Speed droop is favored when the governor is equipped with a mechanical sensing element rather than an electrical one (when both possessing the same equilibrium curves and initial operating points), while the recovery period worsens. On the other hand, two-pulse sensing elements prove even more satisfactory due to their dependence on the angular acceleration term, which is of great importance during transient operation, but may lead to slight instability at the final operating condition, as was documented in Figure 3.16.
- Instantaneous maximum speed droop improves, *i.e.,* it is lower, with higher amplification in the servomechanism, though at the expense of final speed instability; it also improves with higher values of the number and mass of flyweights $(nm)_{fw}$, sensing element spring stiffness k and sensing element spring prior tension y, which lead to initial conditions close to the maximum spring deformation.
- The recovery period deteriorates with smaller values of the mass and number of flyweights $(nm)_{fw}$, low values of P-I element spring stiffness (or higher values of P-I element spring friction coefficients for the vanishing feedback governor) and extremely high amplification, though the trend is not always monotonic.
- The servopiston surface area, the density of the oil used and the differential pressure of the servomechanism all have a marginal effect on the transient response of the engine.

3.3 Friction

3.3.1 Friction Fundamentals

Frictional energy losses inside an internal combustion engine arise from the shearing of oil films between the various working surfaces, *e.g.,* between piston rings and cylinder liner or inside the journal bearings; friction is, thus, interrelated with lubrication. Friction energy is ultimately removed as wasted heat by the cooling system of the engine. The interest in determining friction losses in engines

has increased recently owing to the global requirements for lower fuel consumption and decreased CO_2 emissions, but also for increased engine durability. A detailed review of steady-state engine friction can be found in Ferguson and Kirkpatrick [11] and Heywood [12]. In this book, only some basic aspects will be discussed that deal with the peculiarities of friction development during transient operation.

An important aspect of friction theory is the mode of lubrication, which, as shown in Figure 3.18, can be hydrodynamic, mixed or boundary. In hydrodynamic friction, the surfaces are separated by a liquid film, minimizing the respective wear. This is the desired lubrication mode during engine operation. As pressure increases or speed decreases, oil film thins out to the point where its thickness is comparable in size to the surface irregularities. This is the mixed lubrication regime. With further increase in load or decrease in speed, the boundary layer regime is reached, which, for internal combustion engine applications, is experienced, for example, around dead centers for piston rings. In Figure 3.18, the Stribeck variable is equal to $\mu N/p$, with μ the lubricant dynamic viscosity, N the relative speed between the two surfaces, and p the normal stress. The ordinate in Figure 3.18 is the friction coefficient, defined as the ratio of shear or tangential stress to normal stress acting on a surface.

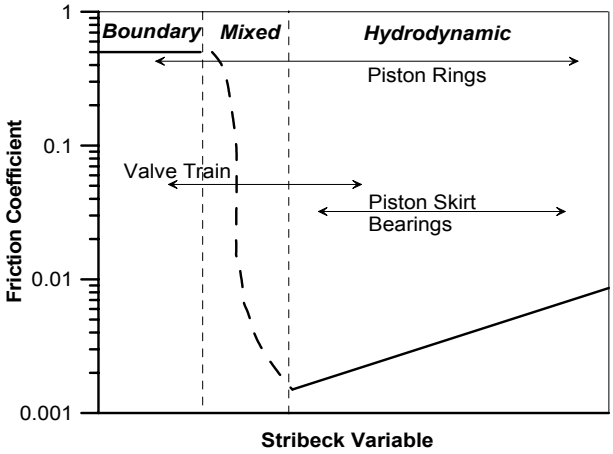

Figure 3.18. Stribeck diagram of friction coefficients for various internal combustion engine components

Engine friction losses comprise of: 1. mechanical friction and 2. accessories work (oil-, water-, fuel pumps, alternators, gears, *etc.*). Following Gish *et al.* [13] in this book, pumping losses are accounted for in the engine bmep by adding both closed and open parts' work and not in the frictional losses.

Mechanical friction occurs in

- piston assembly, consisting of compression and oil rings, and piston skirt;
- valve train; and
- loaded (main crankshaft and connecting rod) bearings.

Around 40–55% of total friction losses in a diesel engine are attributed to the piston assembly friction, 20–30% to loaded bearings, 10–15% to valve train, whereas 15–25% is due to engine auxiliary losses. Piston assembly is dominated by the rings friction contribution. Ring assembly lubrication is, mainly, hydrodynamic, except near dead centers where the oil film breaks down and mixed or even boundary (at firing TDC) lubrication is established. Piston skirt friction losses are generally much lower since the skirt is separated from the cylinder liner by a relatively thick oil film and the gas pressure load has already been largely carried out by the rings; lubrication is here hydrodynamic. Lubrication in the valve train is both boundary and mixed, with the respective frictional losses occurring at the cam-tappet interface, camshaft bearings, valve guides and seals, and at the rocker arm–fulcrum contact. Hydrodynamic lubrication is established in loaded bearings, with mixed conditions assumed around firing TDC, where loading increases considerably. Finally, auxiliary mechanical losses are, mainly, proportional to engine speed.

Ultimately, engine friction reduces the work produced by the thermodynamic gas processes inside the cylinder, and can therefore be calculated from the difference between indicated and brake work as it is described in the following equation on a fmep (friction mean effective pressure) basis

$$\text{fmep} = \text{imep} - \text{bmep} \tag{3.25}$$

For the calculation of engine friction, the following three approaches have been applied [14–17]:

1. global evaluation of mean, over the engine cycle, fmep equations;
2. evaluation of separate mean fmep equations for each component (bearings, valve train, *etc*.) mentioned above; and
3. evaluation of instantaneous friction components contribution at each degree crank angle.

In the first approach, which is the most frequently applied, use is made of the following general type equation:

$$\text{fmep} = \alpha + \beta\, p_{max} + \gamma \bar{u}_{pist} \tag{3.26}$$

where p_{max} is the peak cylinder pressure, $\bar{u}_{pist} = S \cdot N / 30$ is the mean piston velocity, and α, β and γ are constants specific for each engine that are derived after calibration against experimental data at steady-state conditions.

However, it is a well-known fact that friction torque varies significantly during an engine cycle (Figure 3.19); its magnitude compared with brake torque is not negligible, particularly at low loads where the most demanding transient events commence. Modeling of friction is, however, difficult due to the interchanging nature of lubrication and the large number of components that cannot easily be isolated, experimentally investigated, and studied separately even at steady-state conditions.

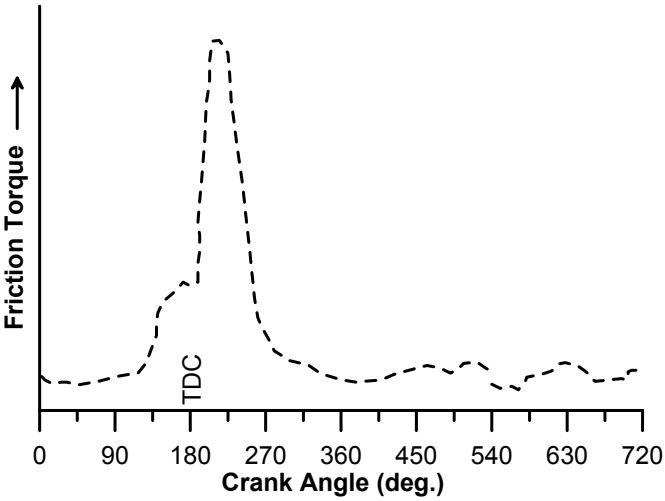

Figure 3.19. Instantaneous friction torque during an engine cycle

3.3.2 Development of Friction Torque during Transients

Many techniques of varying accuracy and complexity have been employed so far for measuring mean friction torque over an engine cycle at steady-state conditions. The most usual ones are: motoring method (here, with partial engine disassembly the distribution of individual components friction can be also estimated), Willans line (extrapolation of bmep *vs.* fuel flow lines to the point of zero fueling), Morse test (one cylinder in a multi-cylinder engine is not fired, reducing accordingly the engine total power) and indicator diagram method (subtraction of bmep, as found from dynamometer measurements, from imep, as computed from cylinder pressure measurements). For the continuously variable speed and fueling conditions, however, of a transient event, these techniques cannot be applied. Instead, instantaneous, total (from all components) transient friction torque can be measured, without need for engine modification, using

- a torque-meter (transducer) between engine and load for the instantaneous resistance torque measurement;
- a piezo-electric transducer for in-cylinder pressure measurement;
- an electromagnetic pick-up or shaft encoder for capturing instantaneous engine speed;
- a comprehensive storing and accurate data analyzing system;
- solution of Equation 3.19 for the unknown friction torque term, using the above-mentioned signals after they have been carefully treated and phased, *i.e.,*

$$\tau_{fr}(\varphi) = \tau_e(\varphi) - \tau_L(\varphi) - G_{tot}\frac{d\omega}{dt} \tag{3.27}$$

Solution of Equation 3.27 can be employed for friction torque evaluation at each degree crank angle during steady-state conditions too, as was the case in Figure 3.19.

Since the technical difficulties involved are considerable, unsurprisingly there is a scarcity of experimental results regarding development of (components) friction torque during transients. Figure 3.20, taken from the work of Winterbone and Tennant [18], shows the variation of mean values over an engine cycle for all torque terms of Equation 3.27 during a load acceptance transient event of a six-cylinder, turbocharged, truck diesel engine applying the above-mentioned experimental procedure.

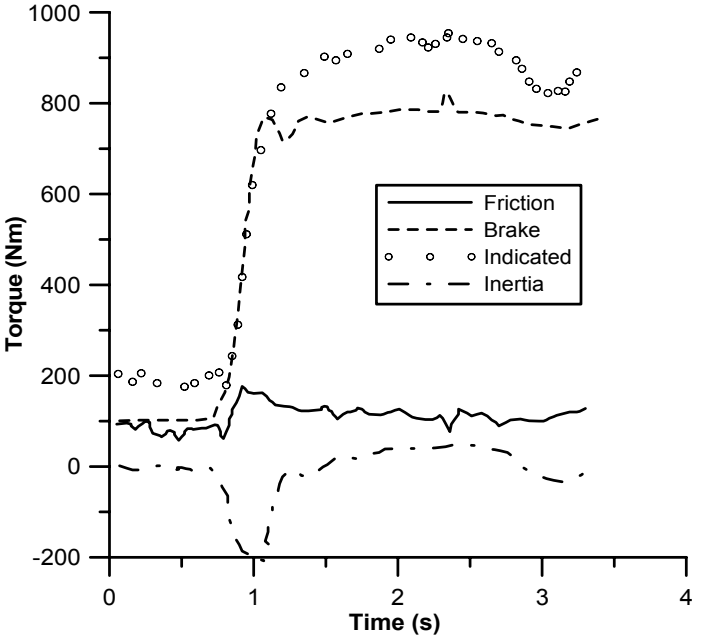

Figure 3.20. Development of mean, over each engine cycle, transient torque terms during acceleration of a turbocharged diesel engine (experimental results reprinted with permission from SAE Paper No. 810339 [18], © 1981 SAE International)

The interesting finding from Figure 3.20 is that the friction torque level overshoots the final steady-state value as the load is applied; this overshoot was estimated between 50 and 100% of the final level of friction. Winterbone and Tennant [18] concluded that during transients, friction is characterized by non-steady-state behavior, differentiating engine response and performance when compared with the corresponding steady-state values predicted by Equation 3.26. Consequently, they proposed that friction torque should generally be overestimated by some percentage during the transient event to account for the peculiarities of transient operation.

The postulated reasons for the apparent increase in friction during transients are

- during the first cycles of the transient event, oil temperature is still low (lower than at the corresponding steady-state operation for the same fueling and engine speed) resulting in higher friction losses compared with steady-state conditions (*cf.* Figure 9.10 for the effects of oil temperature on viscosity, hence friction loss);
- crankshaft deflection is not the same as for the respective steady-state conditions; and
- crankshaft is distorted due to the additional torque being transmitted during both acceleration and deceleration (see also Section 3.4), and also due to the release and absorption of angular momentum stored in the crankshaft mechanism.

Figure 3.21 illustrates the development of the instantaneous upper piston ring friction coefficient during an early cycle of a load increase transient of a turbocharged diesel engine; it refers to simulated results from an experimentally validated transient diesel engine simulation code [1, 19] incorporating a detailed (on a degree crank angle basis) friction model. It is observed that the period of mixed lubrication lasts longer around firing TDC than around the other three dead centers in the cycle. This is due to the increased piston ring friction force F_{PRA} resulting from increased gas pressures during the closed part of the cycle. The important finding from Figure 3.21 is that the friction coefficient development (profile *and* absolute values) remains practically unaltered for each cycle of the transient event (only the duration of mixed lubrication around firing TDC may increase slightly with increased loading/fueling); the maximum value of friction coefficient is determined by the condition of the wall material boundary lubrication. Thus, the values of the corresponding mean or maximum – over an engine cycle – piston rings friction force or torque during the transient event are determined solely by the mean or maximum gas pressures, respectively.

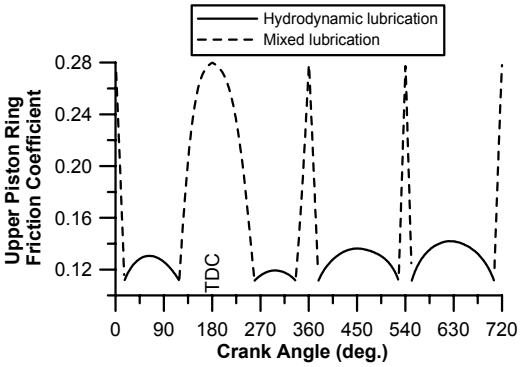

Figure 3.21. Development of upper piston ring friction coefficient during an early cycle of a 10–75% load increase transient event (simulation results)

Figure 3.22 focuses on the development of the reduced transient 'fmep' term, which can be identified as follows:

$$(\text{fmep})_{\text{trans}} = \frac{2\pi \int_{0}^{720} \tau_{\text{fr}}(\varphi)\, d\varphi}{A_{\text{pist}}\, r} \tag{3.28}$$

This fmep response arises from the synergistic effect of gas pressure (through fuel pump rack position response) and engine speed development. Bmep development for cylinder No. 1 of the six-cylinder engine under study is also provided on this figure for comparison purposes.

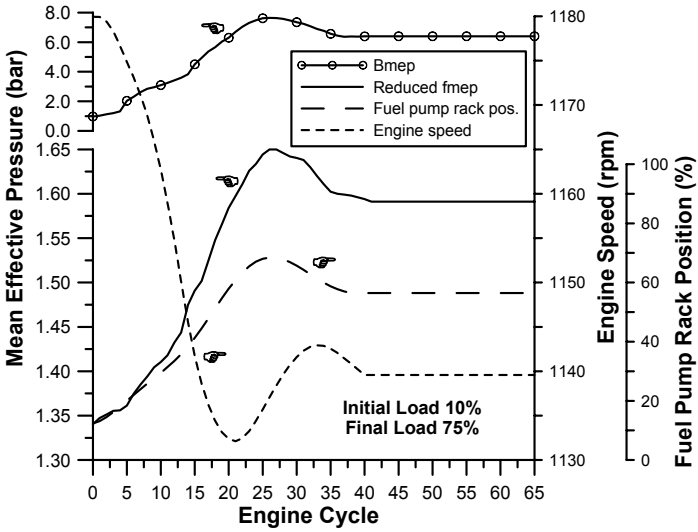

Figure 3.22. 'Reduced' fmep development *vs*. engine cycle for a 10–75% load increase transient event

Loaded bearings and auxiliaries are mostly dependent on engine speed, whereas the impact of gas pressure is dominant for the piston rings assembly. This is highlighted in Figure 3.23, which shows the development of the various friction components' reduced fmep for the same transient load increase of Figure 3.22. The dominance of the piston rings assembly is obvious for the present engine (five piston rings in total, of which the two oil rings each have 6 mm width). An increasing loading, *i.e.,* increased fueling, and hence gas pressures throughout the transient event are responsible for the increase of piston rings friction values. The primary mechanism here is the increase of piston rings and skirt friction forces, although the corresponding values of the Stribeck diagram and friction coefficients behave in an opposite way. On the other hand, piston rings friction force generally decreases with a decrease in engine speed, due to the lower values of mean piston speed as the load increase develops. For the examined transient event, however, the effect of engine speed is modest, owing to the small speed droop observed. All the

other friction terms have smaller contribution to the total transient fmep, especially at the low engine speed under study. This holds, particularly, for the loaded bearings term, which is heavily dependent on engine speed. Only the auxiliaries' friction exhibits a markedly increasing trend during the transient event, due to the significant increase in injected fuel quantity from cycle 15 onwards.

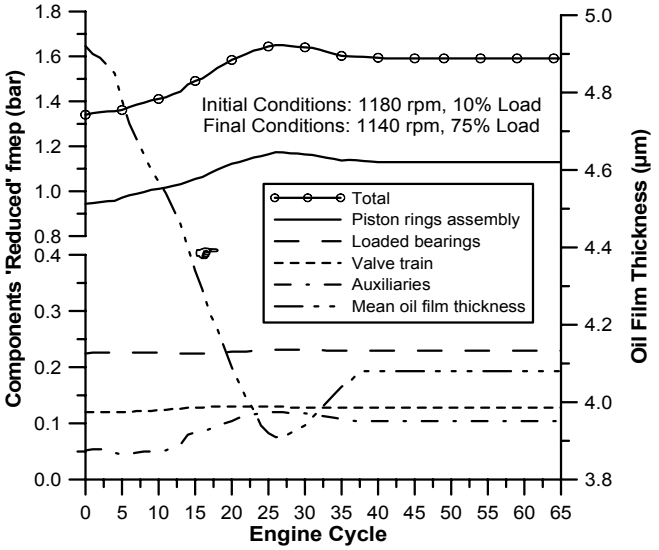

Figure 3.23. 'Reduced' components fmep and mean oil film thickness *vs.* engine cycle for a 10–75% load increase transient event

3.4 Crankshaft Torsional Deformation

An important aspect of internal combustion engine operation is that instantaneous engine torque fluctuates significantly during an engine cycle even under steady-state conditions. The main mechanism behind this is the cyclic nature of gas pressures and inertia reciprocating forces. This fluctuation may be of considerable magnitude, particularly during turbocharged diesel engine operation, where the cylinder pressure assumes very high values. On the other hand, resistance (load) torque remains practically constant during a cycle, owing to the adequately low non-uniformity of rotation; the latter being, mainly, determined by the flywheel mass moment of inertia. As a result, a significant fluctuation occurs in the instantaneous net (engine minus load) torque that eventually leads to cyclic speed irregularities, twists between individual cranks of a multi-cylinder engine and, finally, torsional (angular) deformation of the whole elastic crankshaft affecting also the bearing oil film thickness. Crankshaft deformation is further enhanced during transient operation owing to the dynamic instability induced by the considerable deficit of torque, during the early cycles of the transient event after a

new, increased, load has been applied, or due to the considerable surplus of torque after abrupt fueling increase. With reference to Equations 3.15, the instantaneous torsional deformation of the crankshaft due to the torque difference between engine and load is defined as $(\varphi - \varphi_L)$. Figure 3.24 illustrates the development of crankshaft torsional deformation during typical, steady-state operation of a single-cylinder diesel engine. This figure should be studied in conjunction with Figure 3.25 that depicts the development of all torque contributors during the same engine cycle [20].

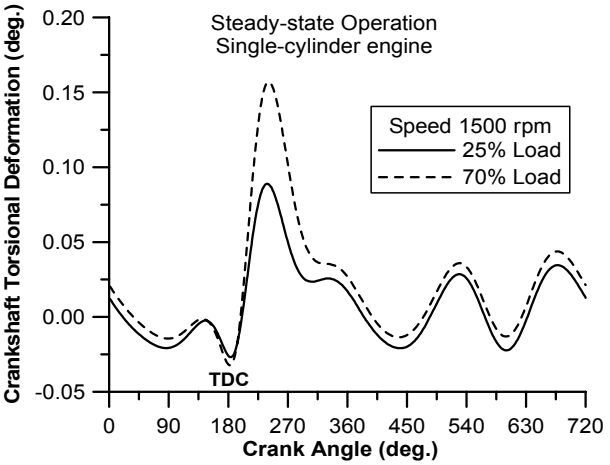

Figure 3.24. Development of crankshaft torsional deformation during steady-state, single-cylinder operation for two different engine loads (simulation results)

During compression (0–180°CA), a deficit of gas torque is observed that leads to engine speed decrease (upper sub-diagram of Figure 3.25) and to the 'negative' crankshaft deformation shown in Figure 3.24; torque, speed and deformation all peak around 'hot' TDC. After the start of combustion, there is a surplus of torque, as now the engine enters the power producing phase of operation. Consequently, 'positive' deformation is established, while the instantaneous engine speed increases. This lasts for the whole expansion stroke. The considerably higher amount of engine torque produced during expansion leads to the greater local peak in crankshaft deformation, *i.e.,* for the present engine 0.16° occurring at about 55°CA after 'hot' TDC, compared with the local minimum of –0.03° at 180°CA (70% load operation in Figure 3.24).

The main mechanism behind the crankshaft torsional deformation profile, over an engine cycle, is clearly the gas torque because of its direct impact on the total engine torque; in fact, Chen and Chen [21] concluded that torsional angle amplitude is, practically, a linear function of the corresponding gas torque. Closer examination of Figure 3.24 reveals that inertia torque influence is also present, mainly during the open part of the cycle where the cylinder pressure is low, as well as during the second half of compression. For the present engine the inertia contribution is rather small, due to the low engine speed (recall from Equation 3.5 that inertia forces vary according to the square of the engine speed).

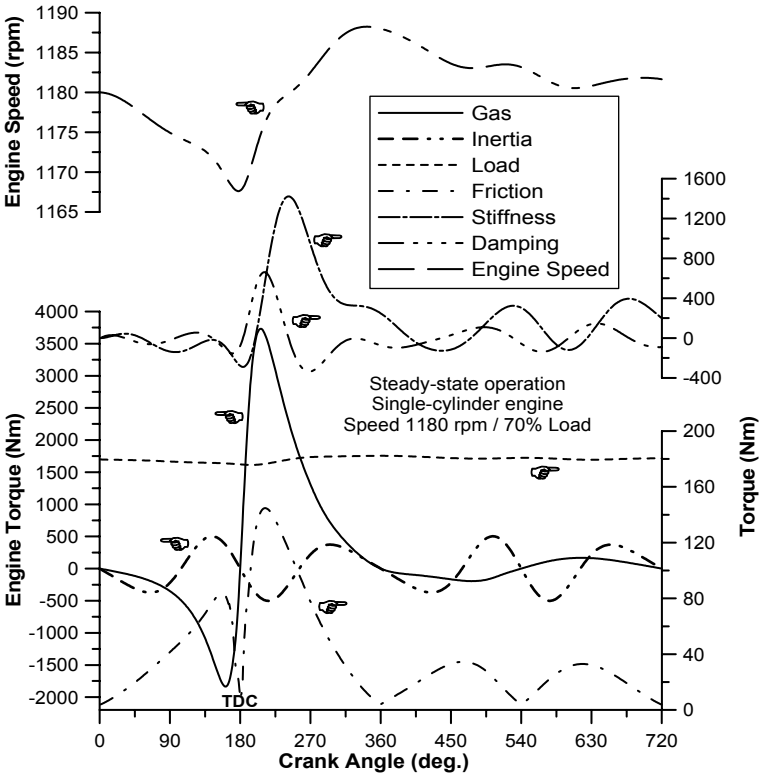

Figure 3.25. Engine speed and various torque contributors build-up during steady-state, single-cylinder engine operation (simulation results)

An interesting finding is that stiffness and damping instantaneous torques may indeed reach high values during an engine cycle. The profile of stiffness torque follows the torsional deformation as dictated by Equation 3.17. The profile of damping torque is indicative of the instantaneous difference between engine and load speeds (ω–ω_L). Owing to the 'internal inertia' of these 'processes', the respective torque peaks observed in the center sub-diagram of Figure 3.25 may be delayed compared with the initiating gas torque or cylinder pressure. However, despite their relatively high instantaneous values, both stiffness and damping torque mean (over the engine cycle) values are negligible compared with their gas or load counterparts.

The torsional deformation for the 25% load is also depicted in Figure 3.24 for comparison purposes. Here, lower maxima of crankshaft deformation are, overall, observed. This was intuitively expected because of the lower values of fueling and consequently engine gas torque produced during this cycle (inertia forces retain the same values as in the 70% load case, since engine speed is the same). Likewise, smaller deformations are experienced in naturally aspirated diesel or in spark ignition engines, where cylinder pressures are much lower. In the latter cases, a

greater influence of inertia torque is also expected, particularly for small SI (automotive) engines operating at high rotational speeds.

Figure 3.26 expands the previous findings to the transient operation illustrating the development of the maximum and the mean, over each engine cycle, deformation and stress for a typical 10–80% load increase transient event of a turbocharged diesel engine.

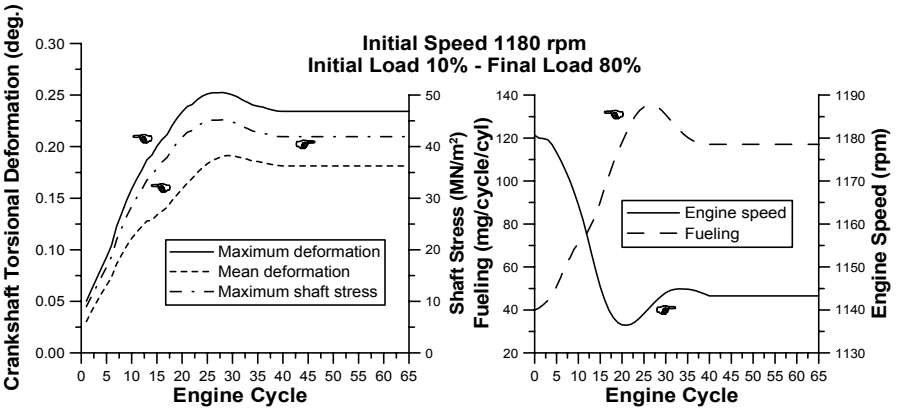

Figure 3.26. Development of the maximum and mean, over an engine cycle, crankshaft torsional deformation and stress during a 10–80% load increase transient event (simulation results)

Initially, the deformation is negligible due to the low engine load (*cf.* Figure 3.24). As the governor responds to the drop in engine speed caused by the abrupt load increase, fueling increases too (right side sub-diagram of Figure 3.26) leading to higher gas pressures and torques throughout the cycle; this results in greater maximum and mean, over the engine cycle, deformations. It is important to note that the instantaneous maximum deformation is considerably higher (up to 50% for the specific engine transient) than the respective mean value in the same cycle; this fact justifies the analysis on a degree crank angle basis, in order to be able to estimate the 'true' maximum stress (left sub-diagram of Figure 3.26) that is instantaneously experienced by the (crank)shaft, *i.e.,*

$$\sigma_{max} = \frac{\Theta}{2}\frac{d}{\ell}\Delta\varphi_{max} = \frac{\Theta}{2}\frac{d}{\ell}(\varphi_e - \varphi_L)_{max} \tag{3.29}$$

where Θ is the shear modulus and d, ℓ are the shaft diameter and length, respectively, between engine flywheel and load (shown in Figure 3.6).

It should be pointed out here that the evolution of transient maximum or mean, over the engine cycle, deformation and, hence, stress develop in a different way compared with the corresponding steady-state engine operation points (*i.e.,* at the same engine speed and fuel pump rack position). The difference is, mainly, attributed to

- the different air–fuel equivalence ratios experienced during transients owing to the turbocharger lag, which significantly affects the air-mass flow-rate, particularly during the early cycles of the transient event; and
- the transient operation of the fuel pump that differentiates from the steady-state fuel pump curves.

The above remarks are expanded in Figure 3.27, by showing the 'wave' of crankshaft deformation build-up for several cycles of a similar transient event. What is interesting here is that the increase in loading/fueling during the transient event leads also to greater in-cycle deformation fluctuations; the respective deformations between individual cylinders are, as expected, much smaller owing to the higher stiffness involved.

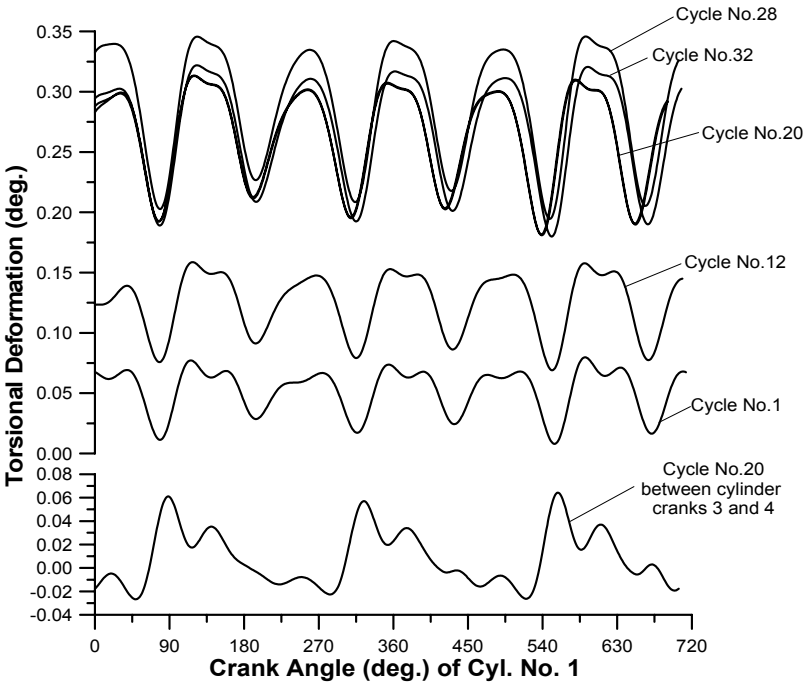

Figure 3.27. Development of torsional deformation between engine and load (upper sub-diagram) and between cylinders 3 and 4 (lower sub-diagram) during various cycles of a six-cylinder engine load increase transient event (simulation results)

3.5 Introduction to Vehicle Dynamics

Application of Transient Cycles for exhaust emission certification of passenger, light and heavy-duty, diesel-engined vehicles has pointed out the importance of studying the transient operation of the whole vehicle and not just of the engine. To this aim, all vehicle's sub-systems need to be properly investigated; the

interconnection between engine, transmission and suspension/tire/road system are of particular importance in determining performance, fuel consumption and exhaust emissions. The latter interconnection induces a much higher degree of complication in the relevant studies (particularly if some kind of hybridization scheme is involved – Section 6.5.4), which need to be extended accordingly in order to account for the various dynamic and control issues incurred.

3.5.1 Simplified Analysis

Figure 3.28 illustrates a simplified engine powertrain module, consisting of the engine, (manual) transmission, final drive-train and wheels; this can be usually considered as an adequate first approximation for engine–vehicle powertrain studies.

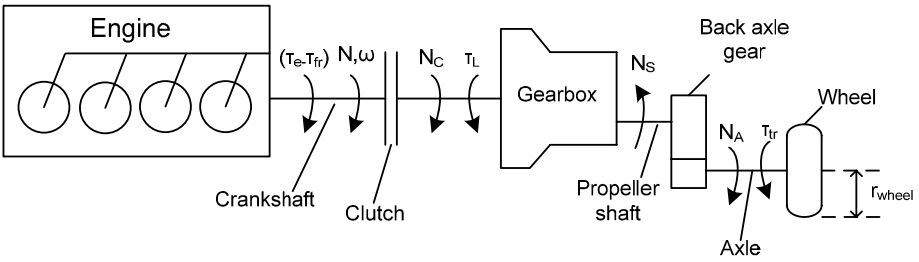

Figure 3.28. Schematic arrangement of simplified engine–gearbox–wheel drivetrain

With reference to Figure 3.28, Newton's second law of motion, expressed on the crankshaft axis, states [22–24]

$$\left[\tau_e(\varphi)-\tau_{fr}(\varphi)\right]-\frac{\tau_L}{\eta_{gear}}=\tau_A=G_V\frac{d\omega}{dt} \tag{3.30}$$

The above relation holds true when the clutch is engaged, *i.e.,* speed N_C equals engine rotational speed N. For the case where the gears are not engaged ($N_C \neq N$), Equation 3.30 is transformed into

$$\frac{\tau_L}{\eta_{gear}}+G_V\frac{d\omega}{dt}=0 \tag{3.30a}$$

In Equation 3.30, engine brake torque $(\tau_e-\tau_{fr})$ is absorbed by the resistances to the vehicle's motion τ_L or by the vehicle acceleration τ_A. Further, we can assume that the various gears (clutch, gearbox, back-axle) absorb another portion of the engine brake torque owing to viscous and mechanical losses; the latter is defined through total gear efficiency η_{gear}. Also, N_S is the speed of the propeller shaft (if applicable), N_A the wheel rotational speed, i_b is the back-axle ratio and i_g the

engaged ratio in the gearbox; the latter ratios are defined as follows with reference to Figure 3.28

$$i_g = \frac{N_C}{N_S} \text{ and } i_b = \frac{N_S}{N_A} \tag{3.31}$$

Instantaneous speed reached by the vehicle is then given by

$$V(\text{km/h}) = 2\pi r_{\text{wheel}} \frac{N_C(\text{rpm})}{i_b\, i_g} \cdot 60 \times 10^{-3} \tag{3.32}$$

The main concern in this kind of study, apart from the correct engine torque evaluation, is the accurate estimation of the various resistances to the vehicle's motion. The three forces, which a vehicle experiences on the road (a fourth term is also present in the more general case where the vehicle tows a trailer), are acceleration dependent inertia force, velocity dependent resistive force, and grade dependent force. Total traction force F_{tr} is given by

$$F_{tr} = F_a + F_r + F_{gr} \tag{3.33}$$

The various terms in Equation 3.33 are defined as follows:

- The aerodynamic force F_a is given by

$$F_a = \frac{1}{2}\rho_\alpha\, c_d\, A_f\, V^2 \tag{3.34a}$$

with A_f the vehicle frontal area, ρ_α the air density and c_d the vehicle aerodynamic resistance (drag) coefficient.

- The rolling resistance force F_r is given by

$$F_r = m_V \left(f + c_{tr} V\right) \tag{3.34b}$$

The latter incorporates the tire rolling resistance (through friction coefficient f), the tire deformation, the friction in the wheel bearing and any other friction elements that are a function of the vehicle motion (defined through vehicle speed V); m_V is the loaded mass of the vehicle.

- The resistance due to road grade is given by

$$F_{gr} = m_V g \sin\theta \tag{3.34c}$$

Grade is defined as the 'rise' over the 'run', being the tangent of the grade angle θ; grade may reach up to 4% in main roads and 10–12% in secondary roads.

For the resistance (traction) torque it holds that $\tau_{tr} = F_{tr}\, r_{wheel}$. This traction torque τ_{tr} needs to be reduced to the crankshaft axis in order to be used in Equation 3.30

$$\tau_L = \tau_{tr}\left(\frac{1}{i_b}\right)\left(\frac{1}{i_g}\right) \tag{3.35}$$

Finally, the vehicle's total moment of inertia, reduced to the crankshaft axis, is given by

$$G_V = m_V\, r_{wheel}^2\left(\frac{1}{i_b}\right)^2\left(\frac{1}{i_g}\right)^2 + G_e + G_{other} \tag{3.36}$$

with G_e the engine moment of inertia as discussed in Section 3.1.3 and G_{other} the inertia of wheels, tires, *etc*. (when reduced to the crankshaft axis). Both G_e and G_{other} terms are usually very small compared with their vehicle mass counterpart, particularly for large vehicles.

Using the previous relations, engine acceleration dω/dt from Equation 3.30 is finally given by

$$\varepsilon = \frac{d\omega}{dt} = \frac{\left(\tau_e - \tau_{fr}\right) - \dfrac{\left(\frac{1}{2}\,\rho_\alpha\, c_d\, A_f V^2 + m_V\left(f + c_{tr} V\right) + m_V\, g\, \sin\theta\right)\left(\frac{1}{i_b\, i_g}\right) r_{wheel}}{\eta_{gear}}}{m_V\, r_{wheel}^2\left(\frac{1}{i_b}\right)^2\left(\frac{1}{i_g}\right)^2 + G_e + G_{var}} \tag{3.37}$$

It is obvious from the above analysis that the lower the engaged gear (this means high i_g), the smaller the total vehicle moment of inertia G_V, resulting in quicker acceleration according to Equation 3.37. On the other hand, the higher the engaged gear, the lower the acceleration rate, but the higher the vehicle speed as calculated from Equation 3.32. The latter remarks can be validated by a numerical example. Typical first gear reduction in a gearbox is around 9 for a 30 tn, 350 kW truck; combined with i_b=5.5 reduction ratio in the rear axle and 0.55 m wheel radius produces a total vehicle mass moment of inertia (excluding engine inertia G_e) $G_V^{1_{st}\,gear} = 30{,}000\cdot(0.55)^2\left(1/9\right)^2\left(1/5.5\right)^2$ = 3.70 kg m^2. The latter is of the same order of magnitude as the engine moment of inertia. For the ninth gear, however, the respective inertia is $G_V^{9_{th}\,gear} = 30{,}000\cdot(0.55)^2\left(1/0.8\right)^2\left(1/5.5\right)^2$ = 468 kg m^2, or almost 130 times the inertia of the first gear.

Various driving modes can be studied using the above-mentioned analysis, *e.g.,* starting the vehicle from rest, shifting into higher or lower gear, climbing a hill,

etc. Winterbone *et al.* [22] discuss some of them; for example, shift into higher gear comprises of

- clutch disengagement and isolation of the engine from the vehicle after the maximum engine speed is achieved; the gear lever is moved to the next higher gear;
- the fuel pump rack is set to its minimum position (when the driver removes his foot from the accelerator pedal). Consequently, the engine decelerates until it reaches a speed equal to the current vehicle speed in the higher gear selected; the vehicle continues to roll, driven by the inertia of the system; and
- the clutch is engaged; the driver fully depresses the accelerator pedal and the rack moves to its maximum position; the engine and vehicle accelerate up to the maximum engine speed.

Figure 3.29 is a typical result of an upward gear change schedule commencing from standstill; it refers to a six-cylinder, turbocharged diesel engine of 11.32 L displacement volume, rated at 175 kW at 1800 rpm, mounted on a 32 t truck with 6.51 m^2 frontal area [22].

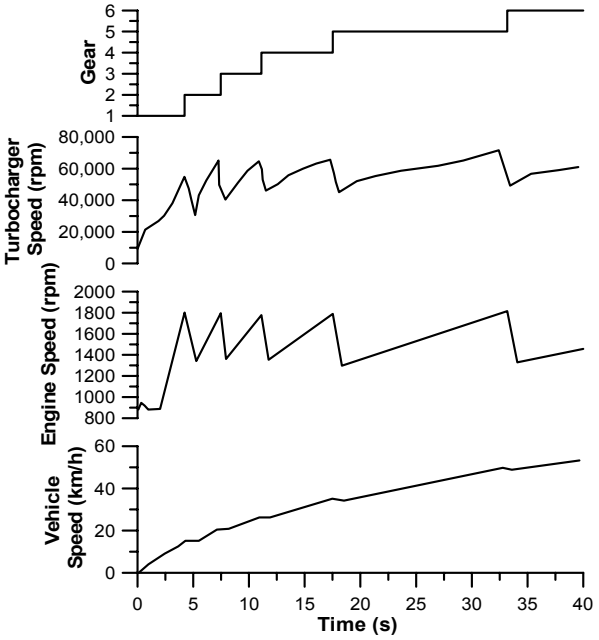

Figure 3.29. Up-gear change schedule of a turbocharged truck (experimental results reprinted with permission from SAE Paper No. 770122 [22], © 1977 SAE International)

The impact of turbocharger lag is here less prominent compared with load acceptance cases of the same engine. This is due to the fact that the acceleration of the engine helps the build-up of boost pressure. The first 5 s are the most critical part of the transient; this interval is influenced by turbocharger lag and system

dynamics significantly more than the rest of the test, since the initial turbocharger speed and available exhaust gas enthalpy are minimal. As a result, smoke emissions are expected to peak during this period too. As the engaged gear increases, so does the inertia of the whole vehicle (Equation 3.36) leading to slower acceleration at higher engine and vehicle speeds.

Interestingly, the study of a similarly rated six-cylinder, two-stroke, turbocharged (with an additional Roots blower prior to the turbocharger compressor) diesel engine of 9 L displacement volume, having 37% more torque than its four-stroke counterpart of Figure 3.29, revealed 43% higher acceleration rate when both engines are installed in the same truck; the comparison concerned sixth gear acceleration [25]. The better response of the two-stroke engined truck was attributed to its Roots blower; the latter's steep pressure ratio *vs.* mass flow characteristics, typical of a positive displacement device (*cf.* Figures 2.5 and 2.7), resulted in an almost immediate rise in engine boost pressure, diminishing turbocharger lag and therefore aiding faster engine and vehicle acceleration.

3.5.2 Detailed Vehicle Dynamics Study

The analysis of Section 3.5.1 does not take into account special vehicle dynamic issues, *e.g.,* suspension effects, multiple driving axles, *etc*. Consequently, the study is engine rather than vehicle oriented. For the latter, more detailed analysis is needed treating the vehicle as separate lumped masses; the lumped mass representing the body is the 'sprung mass', and the wheels and axle masses supported by the tires are denoted as 'unsprung masses'. Such powertrain analyses incorporating detailed vehicle dynamics can be used [24, 26, 27]

- to obtain general vehicle performance data;
- for fuel consumption and exhaust emissions prediction during real driving conditions (gear shift, Transient Cycles);
- as hardware-in-the-loop development tools. An example is in the development of an electronic control module for a powertrain component. Typically, the control module may be simulated in software, and its performance can be assessed by coupling this simulation to the simulated component, *e.g.,* an engine and an engine control module system simulation;
- as vehicle simulators;
- as design tools to assist the design engineer early in the vehicle development process;
- for control system design; and
- for enhancing vehicle driveability.

Owing to the obvious experimental difficulties involved, detailed vehicular transient performance studies have been carried out, mainly, on a simulation basis [28–31] based on a modular modeling philosophy. In the following paragraphs, the analysis will be primarily based on the work conducted by Assanis and co-workers [29, 31]. Although this is not the place to discuss in detail vehicular dynamic issues, a few representative arguments will be made to aid the analysis of the following chapters.

A detailed vehicle dynamic simulation approach includes

1. the engine module describing the in-cylinder and manifolds thermo-dynamic processes;
2. the driveline module consisting of the torque converter, transmission, propeller shafts, differential, and drive shafts; this provides the connection between the engine and the vehicle dynamics module (see Figure 3.30);
3. the vehicle dynamics;
4. traction resistance as already described in Section 3.5.1; and
5. appropriate integration of all the above-mentioned modules.

A typical powertrain system of a 4×2 truck (*i.e.,* vehicle having two axles, the front-one steering and the rear-one driving) is shown in Figure 3.30.

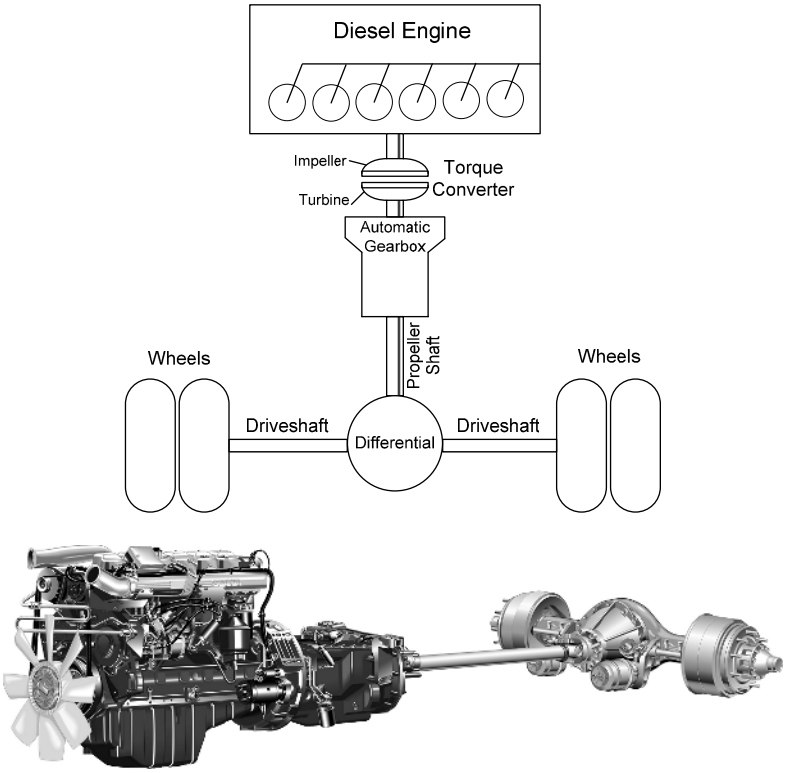

Figure 3.30. *Upper:* Schematic diagram of truck drivertrain with automatic transmission. *Lower:* Drivetrain of a 9 L displacement volume diesel-engined truck (courtesy of Scania CV AB, Illustration: Semcon Informatic Graphic Solutions)

The (turbocharged diesel) engine is connected to the torque converter, whose output shaft is then coupled to the automatic (or automated manual, or continuously variable) gearbox, propeller shaft, differential and two driveshafts, coupling the differential with the driven wheels. For manual gearbox, the engine is directly connected to the transmission via the clutch.

The torque converter input shaft, on the one end, and the wheels, on the other end, are the connecting points for the engine and the vehicle dynamics modules, respectively. The torque converter is usually a fluid coupling, utilizing hydrodynamic principles to amplify the torque input to the transmission at the expense of speed. It consists of an impeller, stator (reactor), and turbine (runner). The impeller is connected to the engine output shaft, and the turbine to the transmission input shaft. The stator is connected to the torque converter housing via a one-way clutch. The presence and arrangement of the stator cause the torque converter to act as a torque multiplication device when operating at low speed ratios, and as an approximately direct-drive fluid coupling at higher speed ratios. The speed ratio is defined as the ratio of turbine speed to impeller speed. The torque converter's output shaft is connected to the automatic transmission with planetary gears. The transmission output torque is multiplied by the transfer case gear ratio to determine the torque transmitted to the differential. The latter determines the acceleration of gears based on propeller shaft torques and inertias. On the one end, the instantaneous shaft speed is determined by the differential output; on the other end, the shaft speed is equal to the wheel speed.

Vehicle dynamics describe the motion of the selected rigid bodies (wheels, axles, suspension and vehicle body) that are allowed to move in space in the longitudinal and heave direction, subject to forces/moments and rigid constraints. A single degree of freedom can be selected in which the vehicle mass is assumed lumped at the center of gravity; such approach is best suited for vehicle acceleration on flat roads. Complexity can be enhanced with more degrees of freedom, as more severe excitations (road roughness, steering, braking, *etc.*) are introduced. This is essential for the investigation of vehicle–powertrain interactions during extreme transients that induce significant pitch motion. The dynamic behavior of sprung and unsprung masses components are coupled through the road/tire interaction. The input to the system is the road profile. The torque from the driveline is applied to the wheel hub, and the available traction force to accelerate the vehicle is affected by the wheel slip. The traction force increases linearly with the wheel slip and it saturates when it reaches a value that is equal to the tire normal force multiplied by the road/tire friction coefficient μ.

Figure 3.31 illustrates the *powertrain integration methodology* of the detailed dynamic vehicle analysis, focusing on the key parameters of each module. One of the main difficulties encountered in such studies is the appropriate link between the engine simulation module with its multi-body vehicle dynamics counterpart. The difficulty arises because of the different time steps required for the solution of the differential equations in each module. The engine module requires a time step of the order of 1°CA, which is much too small for the vehicle dynamics.

The goal of integration is to find the optimum operating mode for the whole powertrain, not just separate parts of it. A major enabling technology in the area of powertrain system integration has been the introduction of CAN (Controller Area Network) bus or similar digital communication links, now almost universally fitted to the vehicle ECUs. Complex time critical control tasks can be distributed among a group of controllers co-operating via such a bus. Various configurations may be employed, and a supervisory controller could govern the separate engine and transmission control systems.

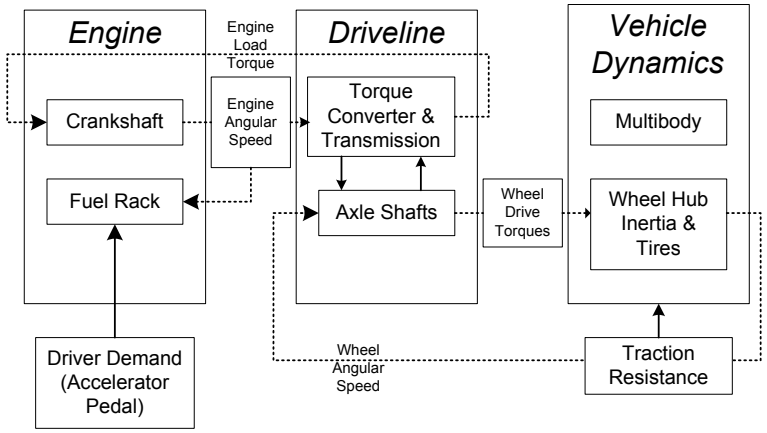

Figure 3.31. Powertrain system integration methodology (adapted from Assanis *et al.* [29])

A typical result from a detailed vehicular modeling approach was reproduced in Figure 1.16 concerning a turbocharged 4×2 truck during the US Highway Driving Cycle.

References

[1] Rakopoulos CD, Giakoumis EG, Dimaratos AM. Evaluation of various dynamic issues during transient operation of turbocharged diesel engine with special reference to friction development. SAE Paper No. 2007-01-0136, 2007.

[2] Lee KS, Assanis DN, Lee J, Chun KM. Measurements and predictions of steady-state and transient stress distributions in a diesel engine cylinder head. SAE Paper No. 1999-01-0973, 1999.

[3] Diesel fuel injection. Stuttgart: Robert Bosch GmbH, 1994.

[4] Krutov VI. Automatic control of internal combustion engines. Moscow: MIR Publishers, 1987.

[5] Welbourn DB, Roberts DK, Fuller RA. Governing of compression-ignition oil engines. Proc Inst Mech Eng 1959;173:575–91.

[6] Webb CR, Janota MS. Governors with load sensing. Proc Inst Mech Eng 1969-70;184:161–74.

[7] Catania AE, Dongiovanni C, Mittica A, Negri C, Spessa E. Study of automotive diesel injection-system dynamics under control. SAE Paper No. 962020, 1996.

[8] Rackmil CI, Blumberg PN, Becker DA, Schuller RR, Garvey DC. A dynamic model of a locomotive diesel engine and electrohydraulic governor. ASME Trans, J Eng Gas Turbines Power 1988;110:405–14.

[9] Zellbeck H, Woschni G. Prediction of the transient response of turbocharged diesel engines. MTZ 1983;44:81–6 (in German).

[10] Rakopoulos CD, Giakoumis EG, Hountalas DT. A simulation analysis of the effect of governor technical characteristics and type on the transient performance of a naturally aspirated IDI diesel engine. SAE Paper No. 970633, SAE Trans, J Engines 1997;106:905–22.

[11] Ferguson CR, Kirkpatrick AT. Internal combustion engines: applied thermosciences, 2nd Edition. New York: Wiley, 2001.
[12] Heywood JB. Internal combustion engine fundamentals. New York: McGraw-Hill, 1988.
[13] Gish RE, McCullough JD, Retzloff JB, Mueller HT. Determination of true engine friction. SAE Paper No. 580063, 1958.
[14] Ciulli E. A review of internal combustion engine losses, pt. 2: studies for global evaluations. Proc Inst Mech Eng, Part D, J Automobile Eng 1993;207:229–40.
[15] Chen SK, Flynn PF. Development of a single cylinder compression ignition research engine. SAE Paper No. 650733, 1965.
[16] Millington BW, Hartles ER. Frictional losses in diesel engines. SAE Paper No. 680590, 1968.
[17] Rezeka SF, Henein NA. A new approach to evaluate instantaneous friction and its components in internal combustion engines. SAE Paper No. 840179, 1984.
[18] Winterbone DE, Tennant DWH. The variation of friction and combustion rates during diesel engine transients. SAE Paper No. 810339, 1981.
[19] Rakopoulos CD, Giakoumis EG. Prediction of friction development during transient diesel engine operation using a detailed model. Int J Vehicle Design 2007;44:143–66.
[20] Giakoumis EG, Rakopoulos CD, Dimaratos AM. Study of crankshaft torsional deformation under steady-state and transient operation of turbocharged diesel engines. Proc Inst Mech Eng, Part K, J Multi-body Dynam, 2008;222:17–30.
[21] Chen SK, Chen S. Engine diagnostics by dynamic shaft measurement: a progress report. SAE Paper No. 932412, 1993.
[22] Winterbone DE, Benson RS, Mortimer AG, Kenyon P, Stotter A. Transient response of turbocharged diesel engines. SAE Paper No. 770122, 1977.
[23] Winterbone DE. Transient Performance. In: Horlock JH, Winterbone DE (eds). The thermodynamics and gas dynamics of internal combustion engines, Vol. II. Oxford: Clarendon Press, 1986;1148–212.
[24] Gillespie TD. Fundamentals of vehicle dynamics. Warrendale PA: SAE International, 1992.
[25] Winterbone DE, Loo WY. A dynamic simulation of a two-stroke turbocharged diesel engine. SAE Paper No. 810337, 1981.
[26] Rubin ZJ, Munns SA, Moskwa JJ. The development of vehicular powertrain system modeling methodologies: philosophy and implementation. SAE Paper No. 971089, 1997.
[27] Jennings MJ, Blumberg PN, Amann RW. A dynamic simulation of the Detroit diesel electronic control system in heavy duty truck powertrains. SAE Paper No. 861959, 1986.
[28] Fluga EC. Modeling of the complete vehicle powertrain using ENTERPRISE. SAE Paper No. 931179, 1993.
[29] Assanis D, Bryzik W, Chalhoub N, Filipi Z, Henein N, Jung D *et al*. Integration and use of diesel engine driveline and vehicle dynamics models for heavy-duty truck simulation. SAE Paper No. 1999-01-0970, 1999.
[30] Assanis D, Filipi Z, Gravante S, Grohnke D, Gui X, Louca L *et al*. Validation and use of SIMULINK integrated, high fidelity, engine-in-vehicle simulation of the international class VI truck. SAE Paper No. 2000-01-0288, 2000.
[31] Filipi Z, Wang Y, Assanis DN. Effect of variable geometry turbine (VGT) on diesel engine and vehicle system transient response. SAE Paper No. 2001-01-1247, 2001.